International Journal of Rock Mechanics & Mining Sciences 127 (2020) 104224

Contents lists available at ScienceDirect

International Journal of Rock Mechanics and Mining Sciences

journal homepage: http://www.elsevier.com/locate/ijrmms

Stress induced permeability changes in brittle fractured porous rock

T.T.N. Nguyen [a], M.N. Vu [b,*], N.H. Tran [a], N.H. Dao [c], D.T. Pham [d]

[a] Le Quy Don Technical University, Institute of Techniques for Special Engineering, Hanoi, Viet Nam
[b] Duy Tan University, Institute of Research & Development, Da Nang, Viet Nam
[c] DrillScan, 26 Rue Emile Decorps, 69100, Villeurbanne, France
[d] Hanoi University of Mining and Geology, Department of Civil Engineering, Hanoi, Viet Nam

ARTICLE INFO

Keywords:
Stress induced permeability change
Wing crack
Percolation threshold
Compression
Effective permeability
Crack closure

ABSTRACT

This paper aims at deriving an approximate model of stress-induced permeability enhancement for brittle cracked porous rock, based on the linear fracture mechanic theory. A recently proposed model of the effective permeability of a porous rock containing an anisotropic distribution of several crack families is used. In such a model, the fluid flow is modelled by Poiseuille's law within the crack and Darcy's law for the porous matrix. The presence of this effective permeability model coupled to an analytical expression of crack growth under shear loading enables the modelling of the permeability variation due to stress-induced cracking in a porous rock. The model is applicable for any initial crack density (*i.e.* lower, around or upper to percolation threshold). Comparisons with experimental results and existing models show the validation and the advantage of the present model. All stages of fluid flow through a cracked porous medium are also reproduced. The proposed model can be easily implemented in a hydromechanical formulation with application to fractured geological formations.

1. Introduction

Rock materials are usually saturated in many geomechanical engineering applications. Thus, the coupled hydromechanical (HM) modelling is essential in order to properly describe their behavior under different type of loadings. In such models, the intrinsic permeability is a key parameter, which is the most significant in the safety analysis of underground nuclear waste repository and CO_2 sequestration. Damage-induced permeability variation changes the pore pressure distribution that in turn affects the mechanical response of the rock through the poromechanical coupling. Experimental studies have evidenced that the material damage process induces a significant permeability change in brittle rocks such as granite,[1,2] sedimentary rocks,[3] claystone.[4]

Two main constitutive models have been proposed to describe the damage induced permeability change: micromechanical and phenomenological models. The phenomenological model is represented by internal variables that are a scalar variable for isotropic damage or second and fourth order tensors for anisotropic damage. The damage evolution law is determined according to the principle of irreversible thermodynamics. This law is implemented in any continuum finite element code for geomechanical application. The post-processing is then performed to formulate the relation between damage variable and permeability, with a focus on stress-induced crack opening[5,6]; crack length growth[7]; crack density distribution[1,8]; pore size distribution change[9] and with the possibility of using empirical laws.[10] The use of a phenomenological approach for a large dimension field scale modelling requires a high computationally cost. On the other hand, the micromechanical approach presents an alternative way to model the damage induced permeability variations.[11,12] This approach allows to link the microstructure modification to the macroscopic properties and to the macroscopic behavior. The effective properties of cracked porous materials are estimated based on the closed-form solution of an individual defect coupling to an approximation schemes to take into account implicitly the interaction between cracks.[13,14] The main features of crack growth, opening and closure, friction, interaction between cracks could be incorporated in such an approach. However, the micromechanical approach is usually used to describe the laboratory test but rarely in engineering applications for field scale modelling. A significant micromechanical model was recently proposed by Chen et al.[15] to describe an anisotropic damage-induced permeability change for crystalline rocks. The authors consider the frictional sliding and dilatancy behaviors of microcracks and the recovery of degraded stiffness when the microcracks are closed. Their model was validated against several experimental results from different brittle rocks. The use of phenomenological and

* Corresponding author.
E-mail address: vungocminh@dtu.edu.vn (M.N. Vu).

https://doi.org/10.1016/j.ijrmms.2020.104224
Received 14 November 2018; Received in revised form 15 January 2020; Accepted 17 January 2020
Available online 24 January 2020

micromechanical models presents a different trend with respect to numerical study of fluid flow through a fractured porous media around beyond the percolation threshold.

The linear fracture mechanic has been rarely used to predict the permeability change for the brittle porous material. Geomaterials are usually subjected to compressive stresses. Therefore, sliding wing cracks seem to be the principal propagation mode of microcracks, which has been proved by both theoretical and experiment studies.[16–19] Simpson et al.[20,21] approximated a wing crack by an equivalent straight crack. The authors proposed analytical expressions for predicting the permeability enhancement due to stress-induced microcracking of rock. In those studies, the authors assumed that the rock medium contains an initial isotropic distribution with fully connected cracks of identical size. However in reality, an initially damaged rock formation could present a distribution of cracks in one or several preferential directions. The crack distribution can be also spread out. For instance, the case of fault zone structure, the damaged zone relatively far from the fault core contains a weak crack density.[22–25] When this zone is loaded by a deviatoric stress, the cracks with favorable orientation grow under wing crack form. This forms a percolated crack network and thus leads to a considerably increase in permeability. Modelling this process is the motivation of this work.

The present work focuses on deriving an approximate model of permeability evolution under compressive stress for a porous rock embedding an anisotropic distribution of cracks, *i.e.* there are several crack families with different orientations. Each crack family is represented by different average parameters, namely orientation, length, hydraulic conductivity and a crack density defined by a number of cracks within a unit area. The closed form model of effective permeability was recently derived for such a fractured porous medium (2D and 3D) based on singular integral equation and homogenization approach.[26–29] In such a model, the interaction between cracks is implicitly taken into account by a self-consistent scheme, which exhibits a percolation threshold for any type of crack distribution apart from a parallel crack repartition. The mass exchange between porous matrix and cracks was explicitly established at an intersection point between two or more cracks.[30–32] Other significant analytical models dealing with the effective permeability of fractured porous media have been developed in 3D configuration.[33,34] The theoretical crack growth model developed by Lehner and Kachanov[17] helps to relate the fracture mechanic to the permeability evolution under compression. The compressive stress induces the propagation of a pre-exiting crack under a wing crack form, whose geometrical parameters (length, orientation and average opening) are explicitly expressed as a function of applied stress. A wing crack system contains three intersecting cracks: initial and two kinked cracks. We consider these three intersecting cracks as three individual cracks and their interaction is implicitly considered via the self-consistent scheme. Simpson et al.[20,21]'s approximation of wing crack system as an equivalent straight crack is also analysed and compared to the present approach. Hence, each crack with favorable orientation grows to create two new parallel cracks from its extremities. In other words, a new crack family of 2*N* cracks could be generated by a pre-existing family of *N* parent cracks. The new crack families with known geometrical and physical parameters corresponding to applied stress are introduced to the initial crack distribution. The comparisons with experimental results on numerous brittle rocks and with micromechanical and phenomenological models were made to validate and to show the advances of the proposed model. The model drawbacks are also discussed.

The present model is practically interesting for geomechanical engineering application, since only poroelasticity is needed for damaged zone. Moreover, it can be easily implemented into any (thermo)hydromechanical (THM) finite element (FEM) code. The compressive stress induced crack growth leads to a change in the rock properties (elastic modulus, permeability, thermal conductivity via the crack distribution and crack opening). The update of the rock properties during the simulation affects the THM responses of damaged zone and the considered geological structure.

2. Permeability evolution due to crack growth

2.1. Effective permeability

Let us consider a porous domain Ω with a uniform permeability tensor $\boldsymbol{k}$ and containing n crack families. Each family, numbered by i, has N_i cracks which are characterized by an average length $2L_i$, an average orientation $\underline{t}_i$, a density $\rho_i = N_i/\Omega$, and an average hydraulic aperture e_i. The crack is modelled by a zero-thickness straight line. The fluid flow is governed by Darcy's law in the porous host rock and Poisseuille's law along the crack. The crack is assumed to have an infinite transversal permeability, i.e. it does not perturb the flow perpendicular to the crack line. The effective permeability $\boldsymbol{k}^{eff}$ of such a material was shown as a sum of the permeability of parent rock $\boldsymbol{k}$ and the fracture contribution $\boldsymbol{k}^f$.[35]

$$\boldsymbol{k}^{eff} = \boldsymbol{k} + \boldsymbol{k}^f \tag{1}$$

The contribution of cracks to the effective permeability is represented by the total fluid flow transported by all cracks per unit area, which was derived by Vu[36] and Vu et al.[37] using self-consistent effective medium. Herein, the derivation procedure of the permeability model is recapitulated.

The contribution of an individual rectilinear crack to the whole permeability is

$$\Psi = \frac{1}{\Omega}\int_{-L}^{L} q(s)ds(\underline{t}\otimes\underline{t}) \tag{2}$$

where L is the crack half length, $\underline{t}$ the tangential vector of crack, q the flow within the crack and s the curvilinear coordinate, Ω the area of considered domain. Ψ is a tensor and is a function of crack parameters: $\Psi(e,L,\underline{t},\boldsymbol{k})$ (e is the crack opening and $\boldsymbol{k}$ the tensor of permeability of host rock).

Consider a diluted distribution of several crack families. Each crack family i is characterized by average parameters: e_i, L_i, $\underline{t}_i$ and a density $\rho_i = N_i/\Omega$ (N_i is the number of cracks of the family i). The interaction between cracks is negligible for the diluted distribution. Therefore, the contribution of the cracks to the permeability is

$$\boldsymbol{k}^f = N_i\Psi(e_i, L_i, \underline{t}_i, \boldsymbol{k}) = \boldsymbol{\Psi}(\rho_i, e_i, L_i, \underline{t}_i, \boldsymbol{k}) \tag{3}$$

and the effective permeability is

$$\boldsymbol{k}^{eff} = \boldsymbol{k} + \boldsymbol{\Psi}(\rho_i, e_i, L_i, \underline{t}_i, \boldsymbol{k}) \tag{4}$$

The self-consistent scheme consists in replacing the matrix permeability tensor $\boldsymbol{k}$ in the crack contribution $\boldsymbol{k}^f$ in the right-hand side of this equation by the effective permeability tensor $\boldsymbol{k}^{eff}$. This allows to implicitly take into account the crack interaction. Self-consistent scheme yields[33,34]

$$\underline{\underline{k}}^f = \sum_{i=1}^{n}\frac{N_i}{\Omega}\int_{-L_i}^{L_i} q(s)\underline{t}_i ds = \sum_{i=1}^{n}\frac{2\rho'_i c_i\sqrt{|\underline{\underline{k}}^{eff}|}}{2c_i + \pi L_i\sqrt{|\underline{\underline{k}}^{eff}|}}(\underline{t}_i\otimes\underline{t}_i) \tag{5}$$

where $\rho'_i = \rho_i\pi L_i^2$ is the dimensionless density of crack family i and $c_i = \frac{e_i^3}{12f}$ with f an empirical factor to account the crack roughness, $|\underline{\underline{A}}|$ is the determinant of tensor $\underline{\underline{A}}$.

The physical behavior of fluid flow through a cracked porous material is well reproduced by model (5). To illustrate the applicability of the present model, two examples are shown. The first one consists in an isotropic porous rock with permeability $\boldsymbol{k} = k\boldsymbol{\delta}$, which contains a random distribution of equal size cracks. The cracks have the length $2L$

and the same variable c. The dimensionless variable $\eta = c/(kL)$ is introduced. The second one consists in a parallel distribution ($\varphi = 90°$) of cracks.

Fig. 1 shows the variations of dimensionless effective permeability ($k^{'} = k^{eff}/k$ with k^{eff} is a diagonal component of the effective permeability tensor) versus the dimensionless crack density. As observed, model (5) shows that: **(i)** For the random distribution of cracks, the effective permeability gradually increases when crack density is weak; considerably at percolation threshold (for a large value of η) and progressively when crack density is large. **(ii)** There is no percolation threshold for a parallel distribution of cracks. The percolation threshold corresponds to a considerably change in permeability (several orders of magnitude) for a high variable η. For an isotropic distribution of cracks, the percolation threshold $\rho'_c = 2$ (see Fig. 1).

The permeability evolution versus crack density for a porous medium containing two or more crack families with different orientations has a similar trend as an isotropic distribution of cracks. Three stages of the permeability evolution versus crack density for an isotropic distribution of cracks: $\rho < \rho_c$, $\rho \approx \rho_c$, $\rho > \rho_c$ (with ρ_c is the percolation threshold) have been also shown when modelling the fluid flow through fractured porous media by using different numerical methods: finite element method,[38] finite volume method,[39,40] boundary element method[32] and finite different method.[8]

2.2. Crack growth model

Hoek and Bieniawski[19] experimentally showed that a pre-existing crack grows, driven by slip along the crack, under a biaxial compressive stress field to form a "wing crack". This observation has been widely demonstrated theoretically and numerically.[26,27] Let's consider an initial crack of length 2L and unit normal vector $\underline{n}$ submitted to a remote stress field $\boldsymbol{\sigma} = \sigma_1 \underline{e}_1 \otimes \underline{e}_1 + \sigma_2 \underline{e}_2 \otimes \underline{e}_2$ ($\underline{e}_1$ and $\underline{e}_2$ are unit vectors of Cartesian coordinate system) (Fig. 2). The axial stress σ_1 is compressive (negative) and the lateral stress σ_2 can be either compressive or tensile (positive). Lehner and Kachanov[17] proposed a simple but rigorously accurate model to quantify the wing crack parameter geometry for large ranges of loading and of initial crack length. As seen in Fig. 2, an initial crack of favorable orientation $\underline{n} = (\cos\varphi, \sin\varphi)$ grows from its two extremities with a fixed deviation $\omega = 70°$ to a length L_w.

Consider that a wing crack can no longer develop when the stress intensity factor K_I at the wing crack point decreases and reaches the fracture toughness K_{IC} of the rock. An analytical solution proposed by Lehner and Kachanov[17] for the stress intensity factor K_I at wing crack tips is used:

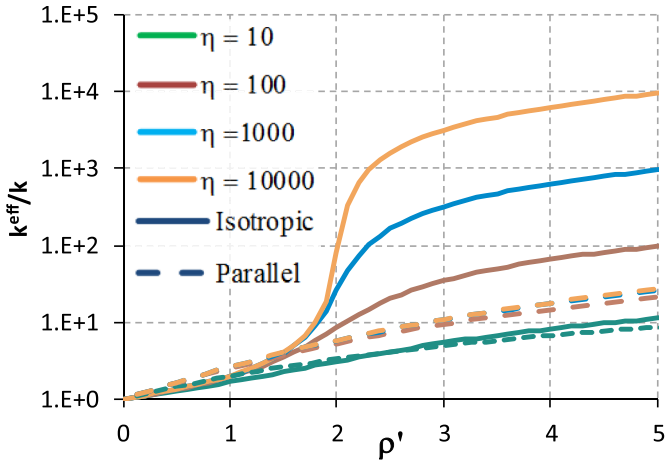

Fig. 1. Effective permeability evolution versus dimensionless density: (a) isotropic distribution of cracks; (b) parallel distribution of cracks.

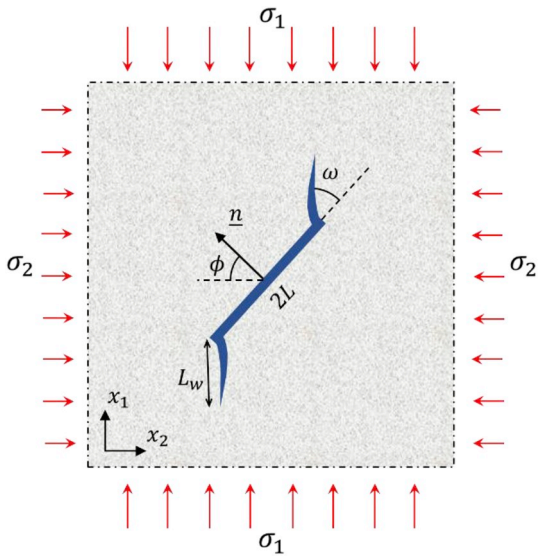

Fig. 2. Winged cracks forming under compressive stress.

$$K_I = \frac{2L\cos\varphi(\tau + \mu\sigma_n)}{\sqrt{\pi(L_w + 3L\pi^{-2}\cos^2\varphi)}} + \sigma_2\sqrt{\pi L_w} \tag{6}$$

where $\tau = |(\sigma_2 - \sigma_1)\sin\varphi\cos\varphi|$ is the shear stress, $\sigma_n = \sigma_1\sin^2\varphi + \sigma_2\cos^2\varphi$ is the normal stress on the initial crack and φ is the angle between two vectors $\underline{e}_1$ and $\underline{n}$.

The kinked crack length L_w is therefore resulted by equating K_I to K_{IC} in Eq. (6), as follows:

$$\frac{1}{S} = -\frac{[-|(1-\lambda)\sin 2\varphi| + \mu(1-\lambda)\cos 2\varphi + \mu(\lambda+1)]\cos\varphi}{\sqrt{\pi^2 l + 3\cos^2\varphi}} - \sqrt{l} \tag{7}$$

where $S = \frac{-\sigma_2\sqrt{\pi L}}{K_{IC}}$ is the dimensionless stress; $l = L_w/L$ is the dimensionless wing crack length; $\lambda = \sigma_1/\sigma_2$is the stress ratio; μ is the friction coefficient of the initial crack.

It should be noted that a positive solution of the dimensionless length l only exists in Eq. (7) for an angle range of $\varphi_1 \le \varphi \le \varphi_2$. Outside this range, cracks are inactive.

Lehner and Kachanov[17] has also given the equation for the sliding displacement of initial crack U as such:

$$\frac{U}{L} = 4\sqrt{2}\,\frac{(\tau + \mu\sigma_n)}{E} + \frac{2\rho(\sqrt{2}-1)}{\cos\varphi}\,\frac{\sigma_2}{E}\,l \tag{8}$$

The wing crack opening at extremities of the initial crack is $U\sin\omega$. According to Jung,[41] the average opening of a wing crack is approximated by:

$$e = \frac{U\sin\omega}{2} \tag{9}$$

Once L_w, e and ω are available, the hydraulic contribution of two wing cracks to the permeability can be calculated by using Eq. (5).

2.3. Stress induced permeability change

2.3.1. Approximation of wing crack system

Consider an initial porous host rock Ω (without loading) embeds in m crack families. Each crack family i is characterized by: a number of cracks N_i, an average length $2L_i$, an average orientation $\underline{t}_i$ (angle φ_i), an average crack aperture e_i (the variable$c_i = \frac{e_i^3}{12f}$) and a crack density $\rho_i = N_i/\Omega$. The total number of cracks within Ω is $N = \sum_{i=1}^{m} N_i$. The initial

permeability of such a medium is determined by Eq. (5).

We assume that there are $m_\varphi \le m$ active families with total $N_\varphi \le N$ cracks, *i.e.* $\varphi_1 \le \varphi_i \le \varphi_2$ corresponding to a considered biaxial loading (σ_1, σ_2). An active crack family i generates a new crack family of $N_{\varphi i} = 2N_i$ wing cracks described by the length L_{wi} determined by Eq. (6) (haft length of the wing crack is $L'_{wi} = L_{wi}/2$); the crack opening e_{wi} calculated by Eq. (9); the orientation $\underline{t}_{wi}$ (φ_{wi} calculated from φ_i and $\omega = 70^\circ$ the angle between the initial crack and the wing crack). The total number of wing cracks is $\sum_{i=1}^{m_\varphi} N_{\varphi i} = 2N_\varphi$. As a result, the effective permeability of the final configuration having $N + 2N_\varphi$ cracks or $m + m_\varphi$ crack families is written as:

$$\underline{\underline{k}}^{eff} = \underline{\underline{k}} + \sum_{i=1}^{m} \frac{N_i}{\Omega} \frac{2\pi L_i^2 c_i \sqrt{|\underline{\underline{k}}^{eff}|}}{2c_i + \pi L_i \sqrt{|\underline{\underline{k}}^{eff}|}} (\underline{t}_i \otimes \underline{t}_i) + \sum_{j=1}^{m_\varphi} \frac{N_{\varphi j}}{\Omega} \frac{2\pi L'^2_{wj} c_{wj} \sqrt{|\underline{\underline{k}}^{eff}|}}{2c_{wj} + \pi L'_{wj} \sqrt{|\underline{\underline{k}}^{eff}|}} (\underline{t}_{wj} \otimes \underline{t}_{wj}) \quad (10)$$

Note that in the effective permeability model (5), L_i is haft length of the parent crack. Therefore, haft length of the wing crack $L'_{wi} = L_{wi}/2$ must be used in Eq. (10) for the effective permeability of the final configuration.

The model described by Eq. (10) exhibits some advances with respect to Simpson et al.[20,21]'s model. Indeed, this model can deal with an evolution from a non-percolated crack network to percolated one due to compressive stress (see Fig. 4) and an anisotropic distribution of several crack families.

The wing crack system consisting of three intersecting cracks presents a strong interaction between the initial crack and two kinked cracks. In the present model, the wing crack is approximated by three individual cracks. The interaction between cracks is implicitly considered by the self-consistent scheme, which is appropriated for a strong interaction configuration.[13] However, the homogenization solution is classically based on the determination of the contribution of a crack to the global permeability by calculation of the flow in a single crack in an infinite matrix. In other words, the flow solution of a wing crack system should be derived and then introduced into Eq. (5), instead of the approximation of the wing crack system as three individual cracks. However, the derivation of the flow solution through a nonrectilinear crack is not a trivial task.

Herein, the approximation of the proposed model is qualitatively analysed. Let's consider a wing crack system in an infinite porous matrix with an isotropic permeability k prescribed at the far field a pressure gradient $\underline{A}$ parallel to the initial crack (Fig. 3). To evaluate the interaction intensity between the initial crack and the kinked cracks, two imagined wing crack systems are added, where kinked cracks grow in the direction perpendicular ($\omega = 90^\circ$) (Fig. 3b) or parallel ($\omega = 0^\circ$) (Fig. 3c) to the initial cracks. As a remainder, the real wing crack corresponds to $\omega = 70^\circ$ (Fig. 3a). With the assumption that the crack does not disturb the flow in the direction perpendicular to it, hence there is no interaction between the kinked cracks and the initial crack for the configuration in Fig. 3b. On the contrary, the case in Fig. 3c seems to present the most important interaction case. For a superconductive crack of length $2a$, the flow within the crack is[35,36]:

$$q(s) = -2k\sqrt{a^2 - s^2}\underline{A}\underline{t} \quad (11)$$

and the total flow is

$$\int_{-a}^{a} q(s)ds = -\pi k a^2 (\underline{t} \otimes \underline{t})\underline{A} \quad (12)$$

The total flow transported by the wing crack system in Fig. 3c is thus $\pi k (L + L_w)^2$. This result is more important than $\pi k L^2 + 2\pi k (L_w/2)^2$ that is the sum of total flow transported by an individual initial crack ($2L$) and two time of total flow within a kinked crack ($2L_w/2$).

It should be expected that the interaction intensity between three intersecting crack increases with a decrease in ω and the real wing crack system with $\omega = 70^\circ$ may be a case where the interaction intensity is far from the case $\omega = 0^\circ$. It must be remembered that the analysis above is for the case where the far-field flow is parallel to the initial crack.

An alternative approach proposed by Simpson et al.[20,21] is to approximate the wing crack system by an equivalent straight crack (Fig. 3d). In this case, the effective permeability becomes

$$\underline{\underline{k}}^{eff} = \underline{\underline{k}} + \sum_{i=1}^{m} \frac{N_i}{\Omega} \frac{2\pi L_{eqi}^2 c_{eqi} \sqrt{|\underline{\underline{k}}^{eff}|}}{2c_{eqi} + \pi L_{eqi} \sqrt{|\underline{\underline{k}}^{eff}|}} (\underline{t}_{eqi} \otimes \underline{t}_{eqi}) \quad (13)$$

The index "*eq*" stands for the equivalent crack. Eq. (5) becomes Eq. (13) if the parameters of initial crack (L_i, c_i, t_i) are replaced by those of equivalent crack (L_{eqi}, c_{eqi}, t_{eqi}). The latter ones can be easily determined from Fig. 3d.[20,21]

However, this approach is not appropriated for an initial distribution of parallel cracks. Indeed, the equivalent crack approach always leads to a parallel distribution of cracks from the initial one. According to Fig. 1, the self-consistent model (5) does exhibit the percolation threshold. The percolation probability of a parallel repartition of cracks is very low even if for a large crack density.[42] In reality, the deviation of kinked crack creates the bridges between initial parallel cracks and forms the fully connected crack network.[41] Moreover, the present approach describes more accurately the global flow direction within the crack network and in the cracked porous rock than the equivalent crack approach. The comparison between the present model and the equivalent crack approach proposed by Simpson et al.[20,21] will be shown again in section 3.

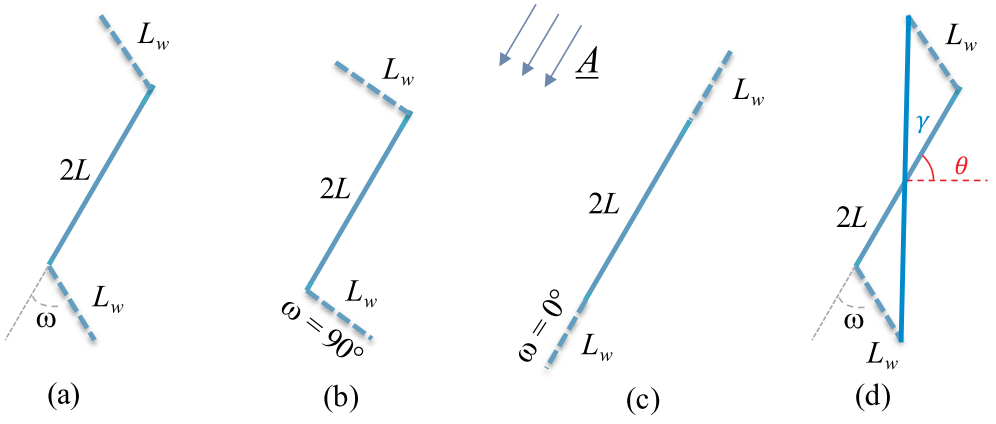

Fig. 3. Wing crack system: (a) $\omega = 70^\circ$ (real wing crack); (b) $\omega = 90^\circ$; (c) $\omega = 0^\circ$; (d) Simpson et al.[20,21]'s equivalent crack.

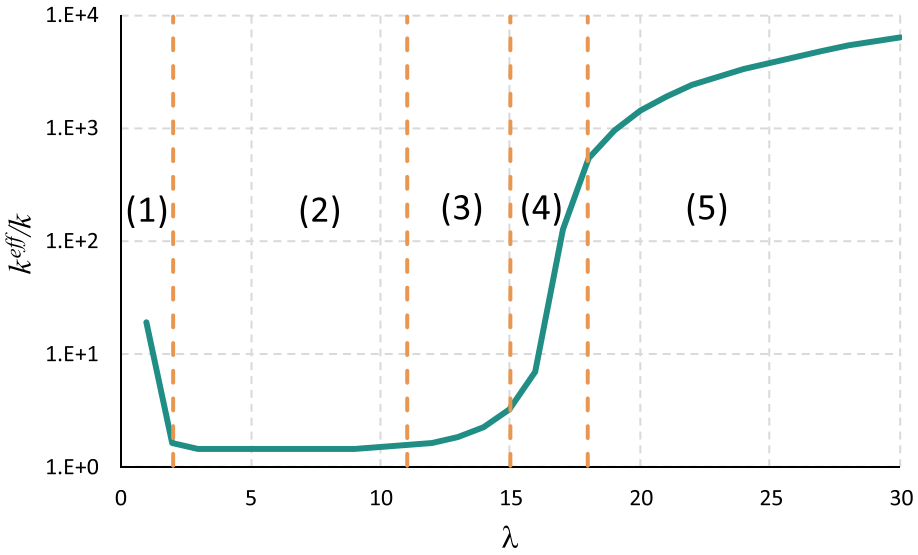

Fig. 4. Stress induced permeability enhancement for a typical case.

Most of experimental results show a decrease in permeability at a lower stress level due to the microcrack closure. This decrease is then normally followed by a constant evolution in permeability until a certain deviatoric stress level. This phenomenon can be modelled using Bandis' law[43]:

$$\sigma_n = K_n \frac{u_n}{\left(1 - \frac{u_n}{u_{max}}\right)^{\gamma}} \tag{14}$$

where $\sigma_n = \sigma_1 \sin^2 \varphi + \sigma_2 \cos^2 \varphi$ is the normal stress on the crack; u_n is the normal displacement; $u_{max} = e_i - e_f$ is the maximum closure of crack; e_i and e_f are respectively the initial and minimum crack apertures; K_n is the normal stiffness and γ is a constant parameter.

2.3.2. Permeability evolution

To illustrate the physics and mechanisms taken into account in the present model, the stress induced permeability change for a representative case is shown in Fig. 4. The rock sample is often initially damaged due to the preparation procedure (coring, conditioning, transport, sample preparation, etc). Thus, a diffuse distribution of cracks (weak crack density) can be present before the test. When submitting to stress, cracks can be closure and growth leading the permeability evolution. A typical change process can be divided into five stages: (1) decrease in permeability due to crack closure (Eq. (14)); (2) constant in permeability when the crack closure reaches e_f and the deviatoric stress level is not large enough to activate the propagation of parent micro-cracks; (3) cracks start growing but the wing crack length L_w in Eq. (10) is still small and this leads to a slow increase in permeability, i.e. the crack network does not percolate in this state and the fluid flow is controlled by both porous matrix and cracks; (4) kinked cracks and pre-existing cracks form a crack network that reaches the percolation threshold corresponding to a dramatically increase in permeability; (5) progressive increase in permeability for large crack density. The crack network percolates and controls essentially the fluid flow.

The percolation threshold corresponds to the total number of cracks (parent and kinked cracks) at the stage (4) in Fig. 4, where $\lambda = \lambda_c$ is known. Three last stages correspond to the three regimes of fluid flow through a fractured porous medium (without mechanical effect), which are described at the end of section 2.1. The typical permeability evolution versus stress, reproduced by the present model, has been often observed during the triaxial test on the brittle rock.[4,7,44–47] Generally, stage (4) corresponds to the peak and the post-peak (softening) of the stress-strain curve, while stage (5) matches the residual behavior. The axial stress decreases within the softening and the residual regimes. However, in some tests, the percolation threshold (some macrocracks result from the coalescence of microcracks) might occur during the pre-peak (hardening) regime.[7,46]

When the sample embeds a percolated crack network, the trend of the stress induced permeability variation depends on the initial distribution of cracks. Fig. 5 presents an example of two crack families initially percolated. The orientations of these two crack families are $\varphi_1 = 65°$ and φ_2. As seen in Fig. 4, the trends of k^{eff}/k versus λ (k^{eff} is a diagonal component of the effective permeability tensor), corresponding to $\varphi_2 = 0°$, 45° and 120°, are different. Indeed, the effective permeability tensor depends on the orientations of existing crack families and induced cracks.

3. Results and discussion

3.1. Comparisons with existing results

This section is dedicated to validate and to highlight the advances of the present model with respect to different micromechanical and phenomenological models by comparing them with experimental data available for different brittle rocks. The equivalent crack approach proposed by Simpson et al.[20,21] (Eq. (13)) is also considered. The measured data of triaxial tests with permeability measurement on Westerly granite and Cerro Cristales granodiorite[47]; Lac du Bonnet granite and Senones granite,[7] Beishan granite[46] are used. For the sake of simplicity, the initial sample is assumed to contains only one parallel crack family that is characterized by an orientation φ_0 and different average parameters: length $2L_0$; initial and minimum apertures e_{i0} and e_{f0}; toughness K_{IC0}; stiffness K_{n0} and constant parameter γ_0 of Eq. (14). The model parameters were calibrated by fitting the data curves k^{eff}/k versus λ. The open source inverse analysis LMFIT[48] is used and adapted to automatically do the calibration procedure. The test confinement on the above rock samples, as well as the calibrated parameters are listed in Table 1. The initial dimensionless crack density $\rho' = \rho\pi L^2$ and the dimensionless crack permeability $k'_f = \frac{e_u^2}{12k}$ are also given in this table. According to Fig. 1, the initial crack distributions are not percolated for five considered samples, since the initial dimensionless crack density varies from 0.4 to 3.6.

We start with the Lac du Bonnet granite since the experiment study of Souley et al.[7] on this material has shown a great interest and used as a reference data test for the elaboration and the validation of several

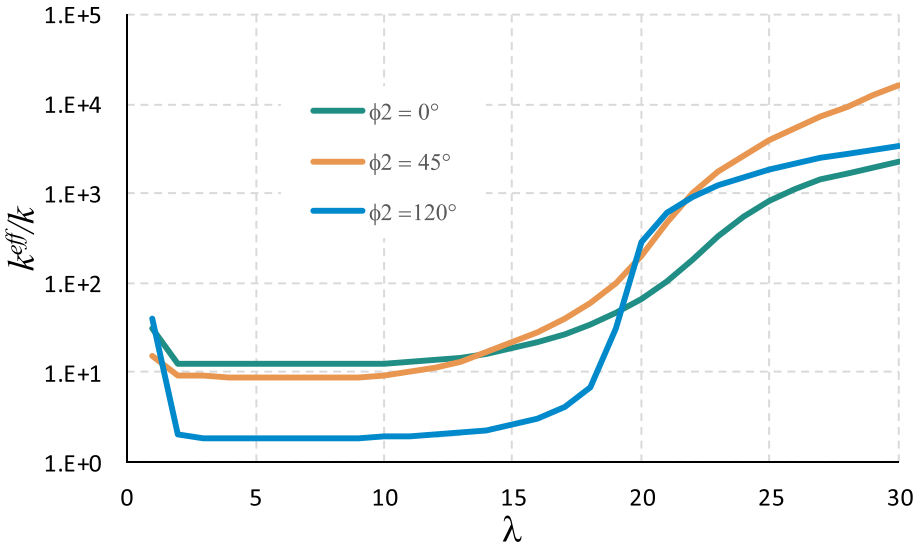

Fig. 5. Stress induced permeability change of a sample initially containing a percolated crack network.

Table 1
Model parameters for five rocks.

Parameters	Lac du Bonnet granite	Senones granite	Beishan granite	Westerly granite	Cerro Cristales granodiorite
Confinement σ_2 (Mpa)	10	5	10	10	5
Number of crack families	1	1	1	1	1
Matrix permeability k (m^2)	5.00E-22	1.30E-19	2.00E-20	6.05E-20	2.00E-21
Crack density ρ (cracks/m^2)	270,000	210,000	80,000,000	210,000	35,000,000
Half of crack length L (m)	0.00085	0.000825	0.00012	0.0008	0.00011
Crack orientation φ (°)	65	50	55	60	47
Initial aperture e_i (m)	2.07E-05	4.00E-05	1.73E-06	3.46E-05	5.00E-06
Utime aperture e_u (m)	1.38E-07	3.46E-06	1.73E-07	3.46E-06	1.15E-07
Stiffness K_n (Mpa)	9.E+08	6.E+08	6.E+08	6.E+08	6.E+08
γ	0.10	0.10	0.10	0.10	0.10
μ	0.60	0.60	0.60	0.60	0.55
S	0.60	0.60	0.60	0.60	0.65
Initial dimensionless crack density $\rho' = \rho\pi L^2$	0.61	0.45	3.62	0.42	1.33
Dimensionless crack permeability $k'_f = \frac{e_u^2}{12k}$	3.17E+06	7.67E+06	1.25E+05	1.65E+07	5.54E+05

phenomenological and micromechanical models.[5,6,12,15] Fig. 6 presents the permeability evolution versus stress parameters λ from test data,[7] the micromechanical model of Chen et al.[15] and the present model. The present model with the equivalent straight crack model represented by

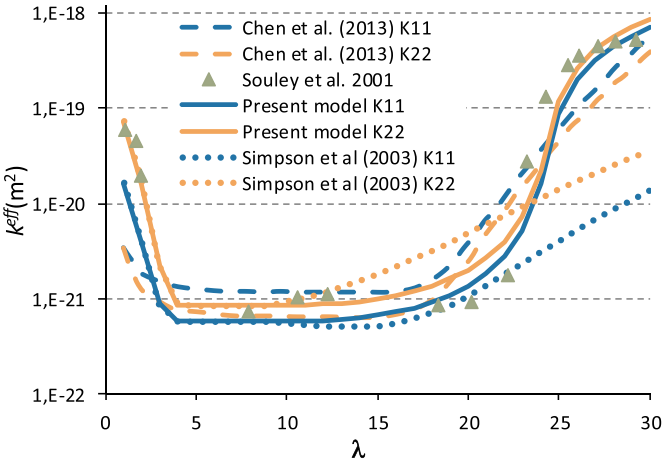

Fig. 6. Microcracking-induced permeability change for Lac du Bonnet granite.

Eq. (13) is also added. The measurement exhibits all five stages of permeability change represented in Fig. 4. As expected, the test data has been reproduced both the trend and the value by the proposed model with only one initial parallel crack family. The introduction of the initial and ultimate crack apertures, incorporated to the crack closure obeying to Bandis' law,[43] helps to present the stages (1) and (2). Whereas, the self-consistent model (10) allows obtaining the stages (3), (4) and (5).

Using the equivalent crack, model (13) does not reveal the percolation threshold. This is due to that only one parallel equivalent crack family is always considered during the compressive loading. Furthermore, the present model reproduces the trend of the data test better than Chen et al.[15]'s micromechanical model. A similar trend to Chen et al.[15] has been also obtained by the micromechanical models of Massart and Selvadurai[6] and Jian et al.,[12] as well as by the phenomenological models proposed by Souley et al.[7] and Shao et al.[5]

If we assume that there are two crack families at the initial state with crack numbers 150000 and 130,000, crack lengths 0.00085 m and 0.00065 m, crack orientations 65° and 25° and other parameters shown in Table 1. Fig. 7 presents the permeability enhancement versus λ derived from Eqs (10) and (13). The two approaches interestingly give a similar trend and close curves. They are in a good agreement with the test data of Souley et al.[7] The equivalent crack approach yields a more pronounced anisotropy in permeability than the present approach. This

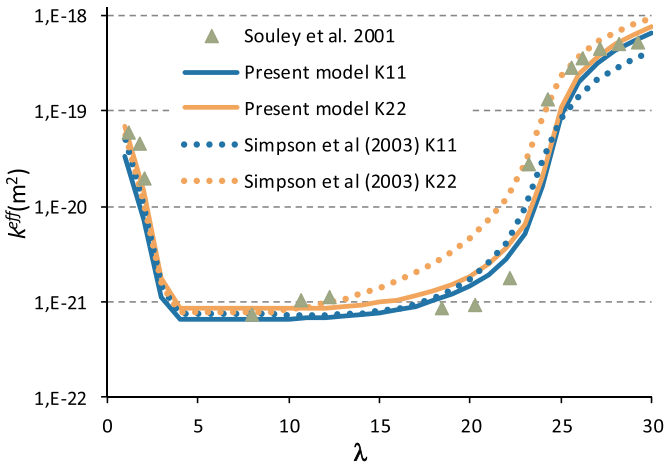

Fig. 7. Two crack families at the initial state: comparison between present and equivalent crack approaches.

comparison could justify the approximation considering the wing crack system as three individual cracks (parent and kinked cracks).

The permeability components K_{11}, K_{22} plotted in Fig. 6 are two diagonal terms of the effective permeability tensor $\boldsymbol{k}^{eff} = K_{ij}\underline{e}_i \otimes \underline{e}_j$ (i,j = 1,2). The off-diagonal term $K_{12} = K_{21}$ is not nil. Fig. 8 illustrates the evolution of the permeability tensor and its eigenvalues (K_1, K_2) normalized by the permeability of the parent rock k. The vertical axis k^{eff}/k can not be represented in log scale since the off-diagonal term deceases and becomes negative when the axial stress increases. In this figure, the percolation threshold is readily sighted where the curve clearly changes the slope. A zoom at the beginning of the curves is also shown in which the vertical axis is represented by log scale for an easy observation. The initial minor eigenvalue is equal to the matrix permeability. Indeed, there is a parallel crack family at the initial stage and the cracks only contribute to the permeability in its tangential orientations. In other words, two eigenvectors of the initial permeability tensor are the normal and the tangent of the crack. The minor and major eigenvalues are respectively the matrix permeability k and the sum of k and the crack contribution.

Comparisons between the experimental data, Chen et al.[15]'s micromechanical model and the present model for other rocks are shown from Figs. 9–12. The measured data showed that the stress induced permeability changes of Beishan granite sample also exhibits all five stages described in Fig. 4. Whereas, it seems that three stages (1), (2) and (3) are observed for Senones granite and Cerro Cristales granodiorite samples and two stages (2) and (3) for Westerly granite. Similarly, the present model is in good accordance with the test data both the trend

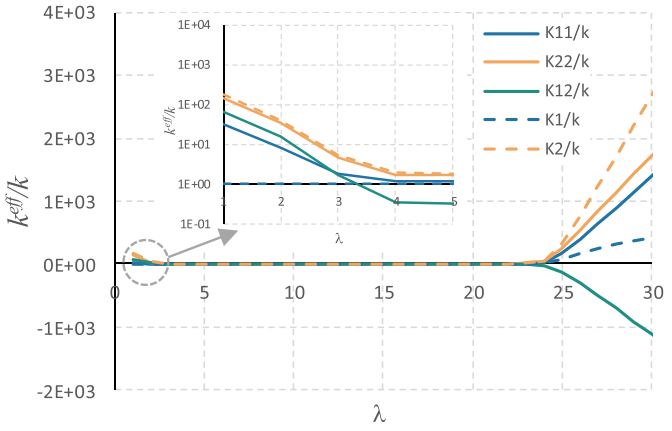

Fig. 8. Evolution of permeability tensor and of its eigenvalues.

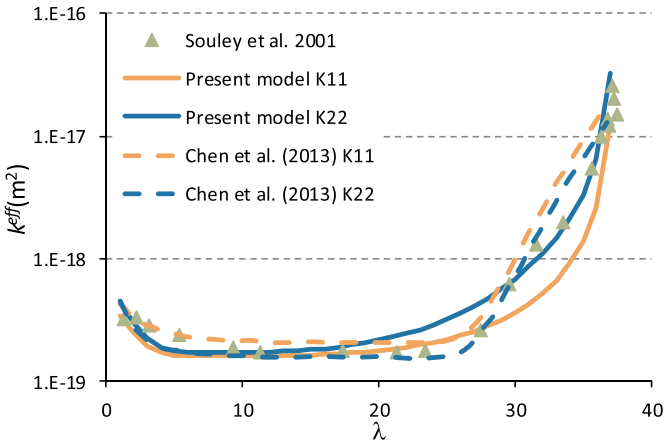

Fig. 9. Microcracking-induced permeability change for Senones granite.

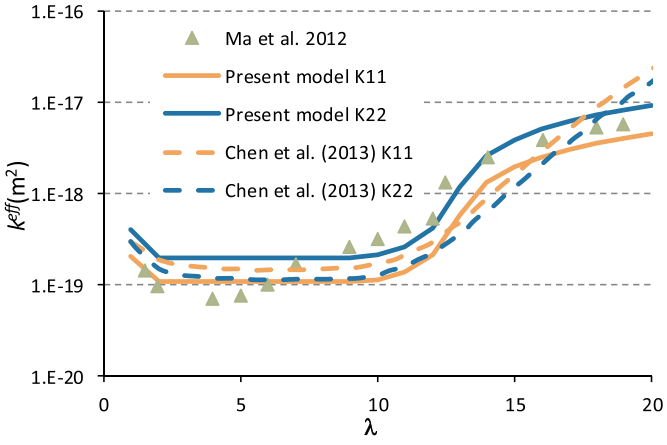

Fig. 10. Microcracking-induced permeability change for Beishan granite.

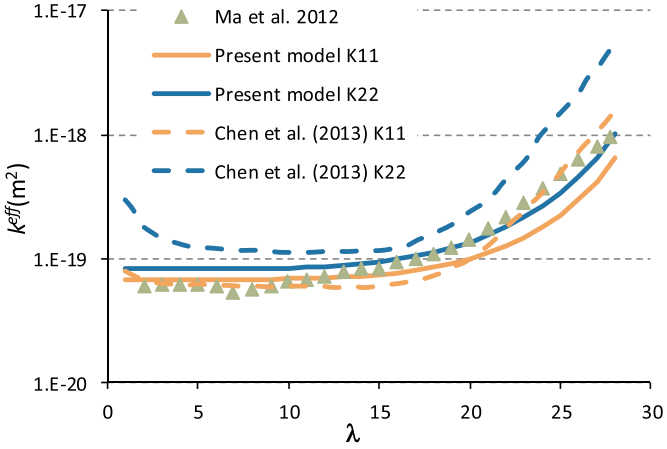

Fig. 11. Microcracking-induced permeability change for Westerly granite.

and the value for Beishan granite. While with this material, the micromechanical model exhibits some difficulties to reproduce accurately the trends. As observed, model (10) are also in good accordance with the test data for other considered brittle rocks.

The triaxial tests considered in this section follow a compression loading paths. As mentioned in section 2.2, the solution of wing crack is right for a compressive axial stress (negative) and an either compressive or tensile lateral stress. Thus, the present model can be used to analyse

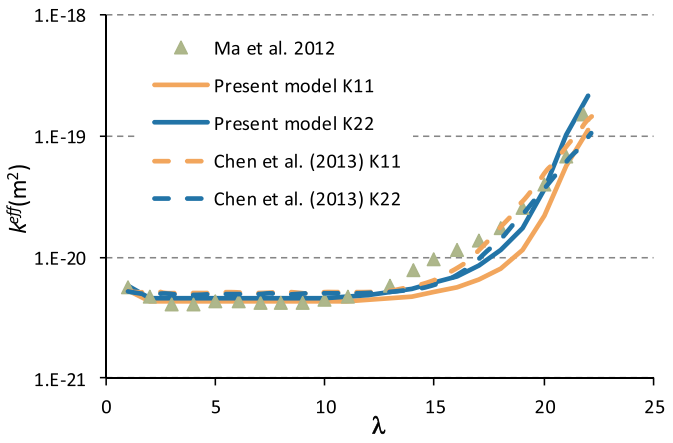

Fig. 12. Microcracking-induced permeability change for Cerro Cristales granodiorite.

the triaxial test under different conditions, for instance extension loading paths.

It is worth reminding that the purpose of this section is not only the calibration but rather the correct reproduction of test data with the assumptions about the crack parameters at the initial state. Indeed, it is hard to determine the microcrack parameters even if the microstructure is available. However, the present model using the assumptions with physical meaning shows: (1) more possibilities in comparison with Simpson et al.[20,21]'s model about the anisotropy of permeability, the crack density at the initial state and the global fluid flow direction within the crack network; (2) a better representation of the trend of the evolution in permeability with respect to micromechanical and phenomenological approaches. The present model is inspired by the physics of the fluid flow through a fractured porous medium as shown in numerical simulations.[8,32,38–40]

3.2. An example of fault core

The present model can be used for a preliminary assessment of the permeability enhancement for a fractured formation when the stress state is known, for instance stress state resulted from a field scale simulation.

The macrocracks present in many geological applications, particularly in fault zones. As an example, in CO_2 storage safety study, the fault core is often considered as a barrier to fluid flow.[49,50] Therefore, the CO_2 injection results in an important suppression in a side of the fault core during the injection phase. This normally leads to an increase in deviator stress. This phenomenon could activate the pre-existing cracks within the fault core and then the permeability considerably increases. In other words, the role of the barrier to fluid flow could not be maintained over the injection of CO_2.

According to Jung,[41] an almost parallel crack distribution is usually observed in the fault core (Fig. 13). The CO_2 injection can induce a great anisotropic compression that activates the crack growth under the wing crack form. Kinked cracks intersecting pre-existing cracks constitute a percolated crack network that considerably increases the permeability of fault core. To show this phenomenon, the permeability enhancement determined by the present model for an initial distribution of a parallel crack family in the fault core is shown. The model parameters are: number of crack family N = 1; crack density ρ = 10 crack/m^2; crack orientation φ = 60°; initial crack aperture e_i = 3.42e-6 m and μ = 0.6. The ultimate aperture is assumed to be equal to the initial aperture ($e_f = e_i = e$), i.e. there is no effect of crack closure on the permeability change (the feature of Eq. (14)) is simply deactivated). The permeability of the fault core matrix is 10^{-20} (m^2).

Fig. 14 plots the variation of three components (K_{11}, K_{22}, K_{12}) of the permeability tensor ($\boldsymbol{k}^{eff} = K_{11}\underline{e}_1 \otimes \underline{e}_1 + K_{22}\underline{e}_2 \otimes \underline{e}_2 + K_{12}\underline{e}_1 \otimes \underline{e}_2 + K_{12}\underline{e}_2 \otimes \underline{e}_1$) as a function of λ for three dimensionless stress S = 0.3, 1 and 5. The value λ_c, at which the percolation threshold occurs, decreases when S increases. Beyond the λ_c, the effective permeability is almost linear to the stress ratio λ. This trend is similar to the numerical results reported by Maleki and Pouya.[8]

For an accurate evaluation of the HM damaged zones' behavior, the approximate model described in section 2 must be implemented into computational tools. This future work may be practically interested in the geomechanical application when dealing with a large dimension field scale simulation, since we only need the poroelasticity. For instance, nuclear waste repository, CO_2 sequestration, where the permeability is the most important parameter for their long-term safety. Indeed, the used of the phenomenological models and the discrete crack model[51,52] are expensive in computational resources and needs a fine mesh to reduce the mesh-sensitive results. Besides, the micromechanical model is not usually in engineering application. The present model can

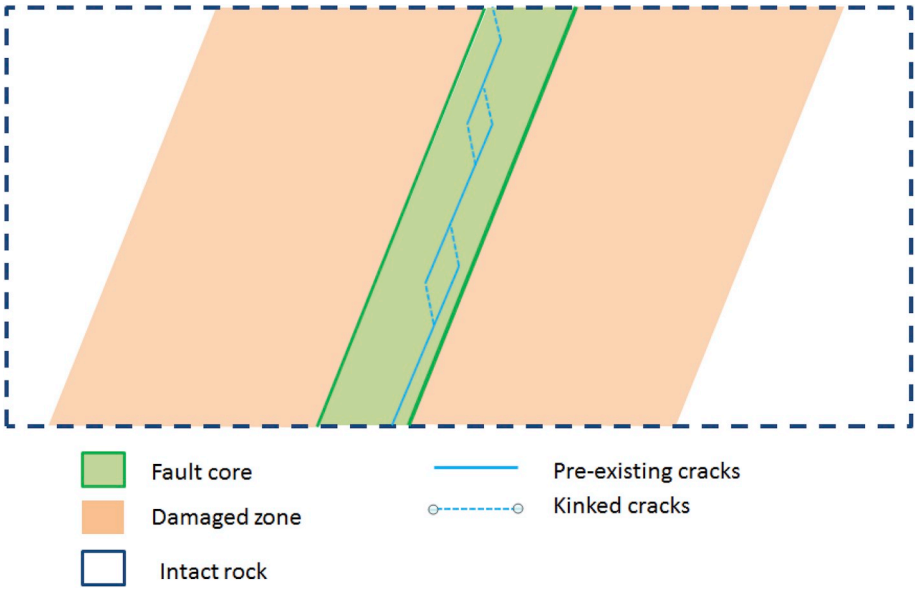

Fig. 13. Crack growth with a fault core under an anisotropic compression.

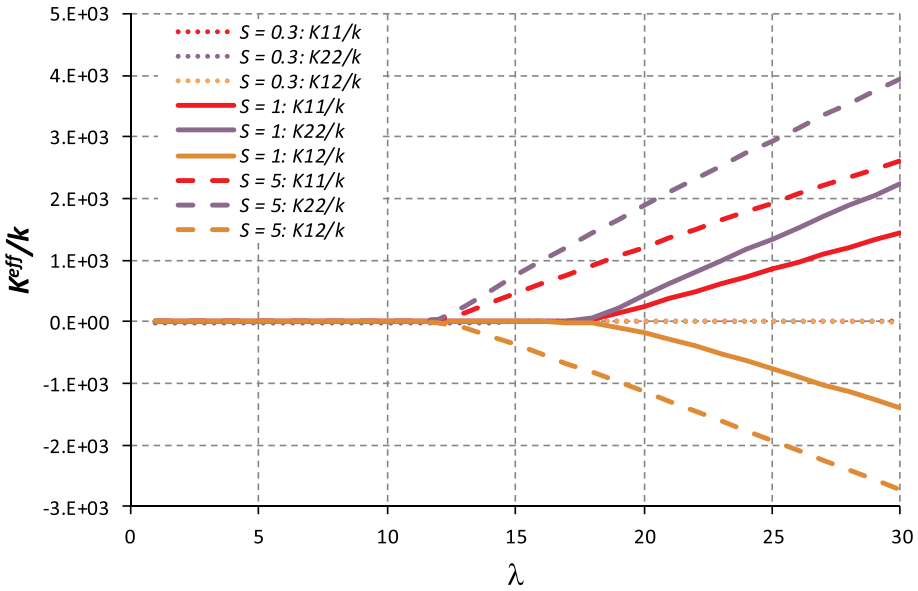

Fig. 14. Stress induced permeability change of a fault core surrounding an initially parallel crack distribution.

be incorporated to a poroelastic modelling, in which the stress field is extracted at each time step to calculate crack parameters and then the effective permeability and the stiffness of the damaged zones and update them for the next time step. This future implementation can be applied to assess more accurately the integrity of CO_2 injection in a deep geological aquifer with the presence of fault zones. The fractures distributions in the fault zone are available in some studies,[23,24,49,50] in which the crack growth induced permeability change has not been taken into account yet. The present model could be also interested in considering the THM of damaged zone during the sliding of fault core (fault reactivation).

3.3. Advantages and limitations of the proposed model

This sub-section is dedicated to recapitulate the advantages, the limitations and the possibilities of improvement of the proposed model.

The present model shows additional possibilities with respect to Simpson et al.[20,21]'s model that is only applicable for an isotropic and fully connected cracks. The proposed model can deal with an anisotropic distribution of cracks at the initial state and any density value (lower, equal or higher than the percolation threshold).

Furthermore, the use of the equivalent crack is a disadvantage for the particular case of a crack family at the initial state, where the percolation threshold does not occur for high stress level. Taking into account the kinked crack orientation also helps to represent better the global direction of fluid flow through cracked porous media.

Besides, the proposed model also reveals some drawbacks that should be improved. Firstly, we consider the wing crack system as three individual rectilinear cracks and use the flow solution of a single crack coupling with the self-consistent scheme, which are not the ordinary homogenization approach. The derivation of the flow solution in and around a single wing crack system is a new challenge for the authors to justify this assumption and/or improve the actual model. Secondly, the calibration of parameters at the initial state is not a trivial task for the case of laboratory sample. However, it exists some data from field estimation of fault zone that the model can use directly. Thirdly, the model presents a monotone relation between stress and permeability. Therefore, the model is only applicable for elastic and hardening (pre-peak) behavior. Finally, the permeability of host rock is constant. However, this limitation can be avoided when implementing the model into a THM FEM code. The permeability of each element can be changed through the porosity that is a function of mechanical variables.

4. Conclusion

This present paper derived an approximate model to predict the permeability variation due to the compressive stress for crystalline rock of low porosity (low permeability matrix). The rock usually contains cracks that can be non-percolated or percolated. Load may induce cracks with favorable orientation with respect to loading direction to be propagated. Under compressive stress, a single crack grows and creates a wing crack system consisting of initial crack and two kinked cracks. All wing cracks systems can form a percolated crack network and increase the permeability of the whole rock.

A closed-form permeability model, based on the self-consistent scheme, is used to determine the effective permeability of a porous rock containing an anisotropic distribution of several crack families. The Linear Elastic Facture Mechanic theory allows to determine the geometry of the kinked cracks of a wing crack system as a function of stress. The kinked cracks are considered as new individual cracks and added to the effective permeability model in order to update the permeability at an applied stress level. This approximation of a wing crack system as three individual cracks are qualitatively justified by considering the interaction intensity between kinked and initial cracks, as well as by comparison with the equivalent crack approximation proposed by Simpson et al.[20,21] The use of Bandis' law for crack closure with the difference between the initial and ultimate apertures allows to model the permeability decrease.

The proposed model shows that the permeability evolution under compressive stress for a typical case includes five steps: (1) Permeability decreases due to crack closure; (2) Permeability remains constant when the ultimate crack aperture is reached; (3) A slight increase in permeability occurs due to the creation of wing cracks; (4) Permeability dramatically increases at percolation threshold; (5) Progressive increase in permeability beyond the percolation threshold. The last three stages correspond to the fluid flow regimes versus crack density through a fractured porous medium, which have been evidenced by different numerical methods. The present model is used to reproduce the test data on several brittle rocks. Depending on the initial state and on the stress range, the test data show all in some cases and a part of the five stages in the other ones. A good agreement between test data and the proposed model for both trend and value is shown. Comparison with micro-mechanical and phenomenological models show a better trend reproduced by the present model when comparing to the test data, in particular, the permeability change around and beyond the percolation

threshold. The model presents some advantages regarding the previous one (Simpson et al.[20,21]) in term of crack distribution and crack density (see section 3.3).

The analytical form of the presented model is easy to implement in a THM computational tool. This must be useful for engineering applications when considering a large geometry field scale model, for example the nuclear waste repository, deep CO_2 geological storage, in which the permeability is the most important parameter. The poroelastic behavior makes possible to deal with the large dimension field scale simulation, in which the stress resulted from each time step is introduced into the proposed model to calculate the permeability and update it for the next time step. Ongoing work focuses on the implementation of this approximate model into a FEM code and use it to study the behavior of the fault zone during the CO2 injection within a deep aquifer.

Declaration of competing interest

The authors declare that they have no known competing financial interests or personal relationships that could have appeared to influence the work reported in this paper.

Acknowledgements

This research was funded by National Foundation for Science and Technology Development (NAFOSTED), Vietnam under grant number 107.01-2017.307. The authors wish to thank the editors and two anonymous reviewers for their constructive comments on earlier versions of this article.

Appendix A. Supplementary data

Supplementary data to this article can be found online at https://doi.org/10.1016/j.ijrmms.2020.104224.

References

1 Oda M, Takemura T, Aoki T. Damage growth and permeability change in triaxial compression tests of Inada granite. *Mech Mater*. 2002;34(6):313–331.
2 Chen Y, Hu S, Wei K, Hu R, Zhou C, Jing L. Experimental characterization and micromechanical modeling of damage-induced permeability variation in Beishan granite. *Int J Rock Mech Min Sci*. 2014;7:64–76.
3 Wang JA, Park HD. Fluid permeability of sedimentary rocks in a complete stress-strain process. *Eng Geol*. 2002;63(3-4):291–300.
4 Zhang CL. The stress-strain-permeability behaviour of clay rock during damage and recompaction. *J. Rock Mech. Geot. Eng.* 2016;8(1):16–26.
5 Shao JF, Zhou H, Chau KT. Coupling between anisotropic damage and permeability variation in brittle rocks. *Int J Numer Anal Methods GeoMech*. 2005;29(12):1231–1247.
6 Massart TJ, Selvadurai APS. Computational modelling of crack-induced permeability evolution in granite with dilatant cracks. *Int J Rock Mech Min Sci*. 2014;70:593–604.
7 Souley M, Homand F, Pepa S, Hoxha D. Damage-induced permeability changes in granite: a case example at the URL in Canada. *Int J Rock Mech Min Sci*. 2001;38(2):297–310.
8 Maleki K, Pouya A. Numerical simulation of damage-Permeability relationship in brittle geomaterials. *Comput Geotech*. 2010;37(5):619–628.
9 Arson C, Pereira JM. Influence of damage on pore size distribution and permeability of rocks. *Int J Numer Anal Methods GeoMech*. 2013;37(8):810–831.
10 Chen W, La Borderie C, Maurel O, Pijaudier-Cabot G, Rey-Bethbeder F. Simulation of damage-permeability coupling for mortar under dynamic loads. *Int J Numer Anal Methods GeoMech*. 2014;38(5):457–474.
11 Zhu Q, Kondo D, Shao J, Pensee V. Micromechanical modelling of anisotropic damage in brittle rocks and application. *Int J Rock Mech Min Sci*. 2008;45(4):467–477.
12 Jiang T, Shao J, Xu W, Zhou C. Experimental investigation and micromechanical analysis of damage and permeability variation in brittle rocks. *Int J Rock Mech Min Sci*. 2010;47(5):703–713.
13 Dormieux L, Kondo D, Ulm F-J. *Microporomechanics*. Wiley; 2006.
14 Nguyen ST, Pham DC, To QD, Vu MN. On the effective transport properties of heterogeneous materials. *Int J Eng Sci*. 2016;104:75–86.
15 Chen Y, Hu S, Zhou C, Jing L. Micromechanical modeling of anisotropic damage-induced permeability variation in crystalline rocks. *Rock Mech Rock Eng*. 2013;47(5):1775–1791.
16 Kachanov ML. A microcrack model of rock inelasticity part II: propagation of microcracks. *Mech Mater*. 1982;1(1):29–41.
17 Lehner F, Kachanov M. On modelling of "winged" cracks forming under compression. In: Bouchaud E, Jeulin D, Prioul C, Roux S, eds. *Physical Aspects of Fracture. NATO Science Series (Series II: Mathematics, Physics and Chemistry)*. vol. 32. Dordrecht: Springer; 2001.
18 Nemat-Nasser S, Horii H. Compression-induced nonplanar crack extension with application to splitting, exfoliation, and rockburst. *J. Geophys. Res. Solid Earth*. 1982;87(B8):6805–6821.
19 Hoek E, Bieniawski ZT. Brittle fracture propagation in rock under compression. *Int J Fract Mech*. 1965;1(3):137–155.
20 Simpson GDH, Guéguen Y, Schneider F. Permeability enhancement due to microcrack dilatancy in the damage regime. *J. Geophys. Res. Solid Earth*. 2001;106(B3):3999–4016.
21 Simpson GDH, Guéguen Y, Schneider F. Analytical model for permeability evolution in microcracking rock. In: Kümpel HJ, ed. *Thermo-Hydro-Mechanical Coupling in Fractured Rock. Pageoph Topical Volumes*. Basel: Birkhäuser; 2003:999–1008.
22 Chester FM, Evans JP, Biegel RL. Internal structure and weakening mechanisms of the san andreas fault. *J. Geophys. Res. Solid Earth*. 1993;98(B1):771–786.
23 Mitchell T, Faulkner D. Towards quantifying the matrix permeability of fault damage zones in low porosity rocks. *Earth Planet Sci Lett*. 2012;339–340:24–31.
24 Seyedi DM, Vu MN, Pouya A. A two-scale hydromechanical model for fault zones accounting for their heterogeneous structure. *Comput Geotech*. 2015;68:8–16.
25 Seyedi D, Ducellier A, Vu MN, Pouya A. A two-scale model for simulating the hydromechanical behavior of faults during CO2 geological storage operation. In: *45th U.S. Rock Mechanics/Geomechanics Symposium*. June 2011:26–29. San Francisco, California.
26 Pouya A, Vu MN. Fluid flow and effective permeability of an infinite matrix containing disc-shaped cracks. *Adv Water Resour*. 2012;42:37–46.
27 Vu MN, Pouya A, Seyedi DM. Modelling of steady-state fluid flow in 3D fractured isotropic porous media: application to effective permeability calculation. *Int J Numer Anal Methods GeoMech*. 2013;37(14):2257–2277.
28 Vu MN, Pouya A, Seyedi DM. Effective permeability of three-dimensional porous media containing anisotropic distributions of oriented elliptical disc-shaped fractures with uniform aperture. *Adv Water Resour*. 2018;118:1–11.
29 Vu MN, Nguyen ST, Vu MH, Tang AM, To VT. Heat conduction and thermal conductivity of 3D cracked media. *Int J Heat Mass Tran*. 2015;89:1119–1126.
30 Pouya A, Vu MN. Numerical modelling of steady-state flow in 2D cracked anisotropic porous media by singular integral equations method. *Transport Porous Media*. 2012;93(3):475–493.
31 Vu MN, Pouya A, Seyedi DM. Theoretical and numerical study of the steady-state flow through finite fractured porous media. *Int J Numer Anal Methods GeoMech*. 2014;38(3):221–235.
32 Vu MN, Nguyen ST, Vu MH. Modeling of fluid flow through fractured porous media by a single boundary integral equation. *Eng Anal Bound Elem*. 2015;59:166–171.
33 Ebigbo A, Lang PS, Paluszny A, Zimmerman RW. Inclusion-based effective medium models for the permeability of a 3D fractured rock mass. *Transport Porous Media*. 2016;113:137–158.
34 Saevic PN, Berre I, Jakobsen M, Lien M. A 3D computational study of effective medium methods. *Applied to Fractured Media. Transp. Porous Media*. 2013;100:115–142.
35 Pouya A, Ghabezloo S. Flow around a crack in a porous matrix and related problems. *Transport Porous Media*. 2010;84(2):511–532.
36 Vu MN. Modélisation des écoulements dans des milieux poreux fracturés par la méthode des équations intégrales singulières. PhD. Thesis. In: *In French. Ecole des Ponts ParisTech*. 2012. France.
37 Vu MN, Nguyen ST, To QD, Dao NH. Theoretical predicting of permeability evolution in damaged rock under compressive stress. *Geophys J Int*. 2017;209(2):1352–1361.
38 Lang PS, Paluszny A, Zimmerman RW. Permeability tensor of three-dimensional fractured porous rock and a comparison to trace map prediction. *J. Geophys. Res. Solid Earth*. 2014;119(8):6288–6307.
39 Bogdanov II , Mourzenko VV, Thovert J-F, Adler PM. Effective permeability of fractured porous media in steady state flow. *Water Resour Res*. 2003;39(1):1–16.
40 Bogdanov II , Mourzenko VV, Thovert J-F, Adler PM. Effective permeability of fractured porous media with power-law distribution of fracture sizes. *Phys Rev E*. 2007;76(3), 036309.
41 Jung R. Egs - goodbye or back to the future. In: Jeffrey R, ed. *Effective and Sustainable Hydraulic Fracturing*. 2013.
42 Adler PM, Thovert J-F. *Fractures and Fracture Networks*. Kluwer Academic; 1999.
43 Bandis S, Lumsden A, Barton N. Fundamentals of rock joint deformation. *Int J Rock Mech Min Sci Geomech Abstr*. 1983;20(6):249–268.
44 Chen Y. Permeability evolution in granite under compressive stress condition. *Geotech Geol Eng*. 2018;36(1):641–647.
45 Wang CP, Wang XY, Chen L, Wang J, Su R, Liu JF. Experimental study on the permeability evolution of granite during complete stress-strain process. In: *International Society for Rock Mechanics and Rock Engineering*. Shanghai, China: ISRM SINOROCK; 18-20 June 2013.
46 Ma L, Wang J, Zhao X, Tham L. Experimental study on permeability of Beishan granite. In: *Rock Mechanics: Achievements and Ambitions - Proceedings of the 2nd ISRM International Young Scholars' Symposium on Rock Mechanics*. 2012:173–176.
47 Mitchell TM, Faulkner DR. Experimental measurements of permeability evolution during triaxial compression of initially intact crystalline rocks and implications for fluid flow in fault zone. *J. Geophys. Res. Solid Earth*. 2008;113(B11). B11412.
48 Lmfit. Non-linear least-squares minimization and curve-fitting for Python. https://lmfit.github.io/lmfit-py/fitting.html.
49 Nguyen TK, Pouya A, Rohmer J. Integrating damage zone heterogeneities based on stochasticrealizations of fracture networks for fault stability analysis. *Int J Rock Mech Min Sci*. 2015;80:325–336.

50 Rohmer J, Nguyen TK, Torabi A. Off-fault shear failure potential enhanced by high-stiff/lowpermeable damage zone during fluid injection in porous reservoirs. *Geophys J Int*. 2015;202(3):1566–1580.
51 Pouya A, Vu MN, Ghabezloo S, Bendjeddou Z. Effective permeability of cracked unsaturated porous materials. *Int J Solid Struct*. 2013;50(20):3297–3307.
52 Pouya A. A finite element method for modeling coupled flow and deformation in porous fractured media. *Int J Numer Anal Methods GeoMech*. 2015;39(16):1836–1852.